



Increasing but Variable Trend of Surface Ozone in the Yangtze River Delta Region of China

Keqin Tang¹, Haoran Zhang¹, Weihang Feng², Hong Liao¹, Jianlin Hu¹ and Nan Li^{1*}

¹Jiangsu Key Laboratory of Atmospheric Environment Monitoring and Pollution Control, Jiangsu Collaborative Innovation Center of Atmospheric Environment and Equipment Technology, School of Environmental Science and Engineering, Nanjing University of Information Science and Technology, Nanjing, China, ²Institute for Atmospheric and Earth System Research, Faculty of Science, University of Helsinki, Helsinki, Finland

OPEN ACCESS

Edited by:

Hongmei Xu,
Xi'an Jiaotong University, China

Reviewed by:

Chunlei Cheng,
Jinan University, China
Qingyan Fu,
Shanghai Environmental Monitoring
Center, China

*Correspondence:

Nan Li
linan@nuist.edu.cn

Specialty section:

This article was submitted to
Atmosphere and Climate,
a section of the journal
Frontiers in Environmental Science

Received: 15 December 2021

Accepted: 10 January 2022

Published: 18 February 2022

Citation:

Tang K, Zhang H, Feng W, Liao H, Hu J
and Li N (2022) Increasing but Variable
Trend of Surface Ozone in the Yangtze
River Delta Region of China.
Front. Environ. Sci. 10:836191.
doi: 10.3389/fenvs.2022.836191

Surface ozone (O₃) increased by ~20% in the Yangtze River Delta (YRD) region of China during 2014–2020, but the aggravating trend is highly variable on interannual time and city-level space scales. Here, we employed multiple air quality observations and numerical simulation to describe the increasing but variable trend of O₃ and to reveal the main driving factors behind it. In 2014–2017, the governmental air pollution control action plan was mostly against PM_{2.5} (mainly to control the emissions of SO₂, NO_x, and primary PM_{2.5}) and effectively reduced the PM_{2.5} concentration by 18%–45%. However, O₃ pollution worsened in the same period with an increasing rate of 4.9 μg m⁻³ yr⁻¹, especially in the Anhui province, where the growth rate even reached 14.7 μg m⁻³ yr⁻¹. After 2018, owing to the coordinated prevention and control of both PM_{2.5} and O₃, volatile organic compound (VOC) emissions in the YRD region has also been controlled with a great concern, and the O₃ aggravating trend in the same period has been obviously alleviated (1.1 μg m⁻³ yr⁻¹). We further combined the precursor concentration and the corresponding O₃ formation regime to explain the observed trend of O₃ in 2014–2020. The leading O₃ formation regime in 2014–2017 is diagnosed as VOC-limited (21%) or mix-limited (58%), with the help of a simulated indicator HCHO/NO_y. Under such condition, the decreasing NO₂ (2.8% yr⁻¹) and increasing VOCs (3.6% yr⁻¹) in 2014–2017 led to a rapid increment of O₃. With the continuous reduction in NO_x emission and further in ambient NO_x/VOCs, the O₃ production regime along the Yangtze River has been shifting from VOC-limited to mix-limited, and after 2018, the mix-limited regime has become the dominant O₃ formation regime for 55% of the YRD cities. Consequently, the decreases of both NO_x (3.3% yr⁻¹) and VOCs (7.7% yr⁻¹) in 2018–2020 obviously slowed down the aggravating trend of O₃. Our study argues that with the implementation of coordinated regional reduction of NO_x and VOCs, an effective O₃ control is emerging in the YRD region.

Keywords: ozone, YRD region, NO₂, O₃ formation regime, WRF-Chem

INTRODUCTION

Tropospheric ozone (O_3) is a critical secondary air pollutant featured with strong oxidation (Thompson, 1992), which is produced via complicated photochemical reactions with volatile organic compounds (VOCs) and nitrogen oxides (NO_x , $x = 1$ and 2) acting as its precursors (Seinfeld and Pandis, 2006; Wang et al., 2017). A high concentration of O_3 may degrade air quality and pose health risks to humans, such as respiratory illness and premature birth (Barry et al., 2019; Ekland et al., 2021; Guan et al., 2021). Moreover, a severe O_3 pollution episode leads to premature mortality as well. A rise of $10 \mu\text{g m}^{-3}$ in O_3 concentration would increase mortality by 2% (Lei et al., 2019). For the ecosystem, O_3 can impair plant production by getting into leaves through stomata (Ainsworth et al., 2012). Agricultural yields are also negatively impacted by O_3 with losses ranging from 6% to 15% for wheat products in China (Feng et al., 2015). At the same time, as an oxidant, the elevated O_3 also promotes the formation of secondary aerosols (Chen et al., 2020b; Feng et al., 2021). For example, the enhanced O_3 and secondary aerosols induced an unexpected haze event in Beijing during the COVID-19 lockdown (Huang et al., 2020; Le et al., 2020).

In 2013, China implemented the Air Pollution Prevention and Control Action Plan (APPCAP), which includes a series of measures for alleviating the current air pollution with particular attention to fine particulate matter ($PM_{2.5}$). The $PM_{2.5}$ pollution was, thus, effectively controlled with more than 30% of nationwide $PM_{2.5}$ reduced by the end of 2018 (Zhai et al., 2019). At the same time, O_3 concentration indicated an inverse trend. The average maximum daily average 8-h O_3 at the 90th percentile (MDA8-90) in 74 major cities increased by 20% from 2013 to 2017 in China. Major causes for the aggravated O_3 are summarized as follows. First, a decrease in NO_x and increase in VOC emissions (Zheng et al., 2018) facilitated the nonlinear production of O_3 in urban areas that belong to VOC-limited (Wang et al., 2017; Li et al., 2019c; Liu and Wang, 2020b). Second, enhanced radiation intensity and increased HO_2 radicals caused by the reduced $PM_{2.5}$ also posed a nonnegligible influence on O_3 pollution (Li et al., 2019a). Besides this, the meteorologically driven variability also contributed to the increase of O_3 (Liu and Wang, 2020a; Dang et al., 2021). From 2013 to 2017, humidity and wind speed drove an annual increase of 2.3 ppbv in O_3 over the Yangtze River Delta (YRD) region (Li et al., 2019b).

The rapid increase of O_3 in China since 2013 has been confirmed by many observational and model studies (Shen et al., 2019; Zhai et al., 2019; Chen et al., 2020c; Shen et al., 2020; Liu et al., 2021; Mousavinezhad et al., 2021). However, the upward trend has significant differences in different regions and different periods. Chen et al. (2021) revealed that annual O_3 concentration was in continuous increase across the YRD region during 2014–2019 but rose in volatility in the Pearl River Delta (PRD) region over the same period. In addition, the increment of O_3 in the YRD region is more obvious with a rate of 3.2 ppbv yr^{-1} from 50.7 to 66.3 ppbv, which is approximately four times that in the PRD region.

In this study, we used multiple air quality observations in conjunction with a regional chemical model, weather research and forecasting coupled with chemistry (WRF-Chem) to analyze the O_3 pollution in the YRD region from 2014 to 2020 with the aim of exploring the interannual and regional variations of O_3 and understanding the chemical principles behind it. Our study differs from previous studies in that 1) we combined surface air quality and meteorology observations, satellite remote sensing observations, numerical model simulation and an indicator-based approach to uncover the increasing but variable pattern of O_3 in the YRD region, and 2) we further explored and compared the chemical mechanisms and driving factors in different regions and at different stages.

MATERIALS AND METHODS

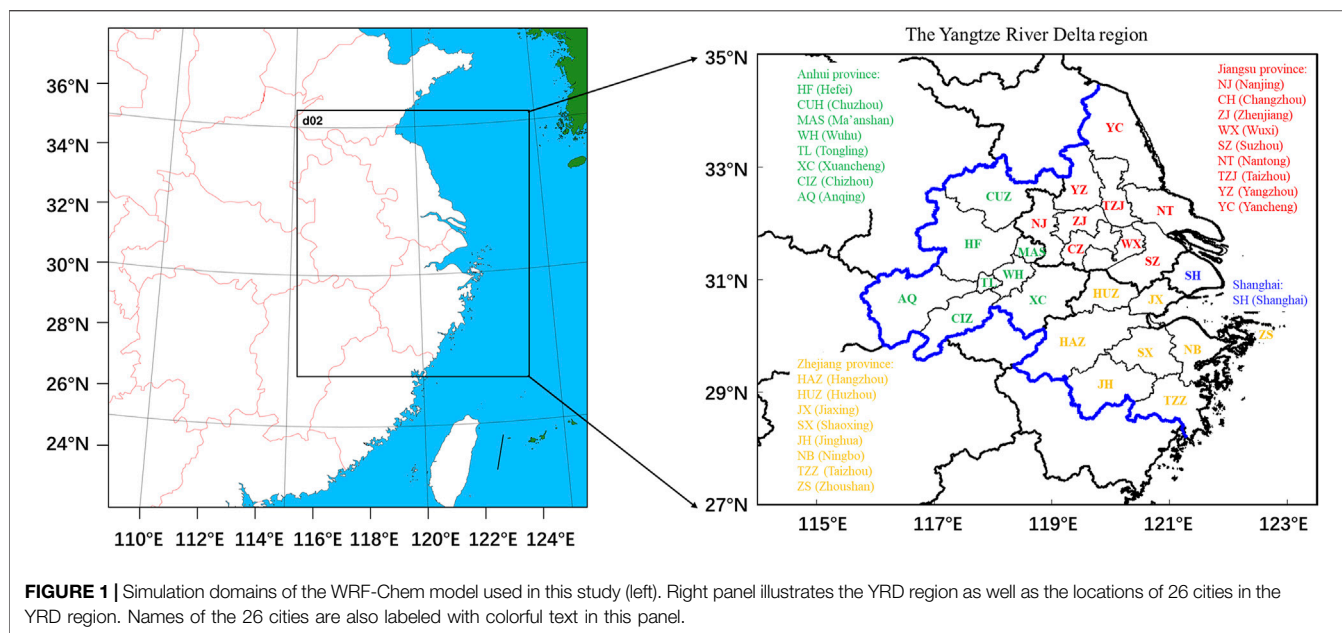
Observation

We adopted air quality monitoring measurements from 2014 to 2020 over the YRD region (Figure 1). Data was derived from the public website of the Ministry of Ecology and Environment (MEE) of China (<http://106.37.208.233:20035/>). MEE provides hourly *in situ* measurements of six criteria air pollutants, including $PM_{2.5}$, PM_{10} , NO_2 , O_3 , SO_2 , and CO. A total of 127 sites from 26 cities in the YRD region were utilized for further analyses. Descriptions for the monitoring sites and cities can be found in **Supplementary Table S1**; **Supplementary Figure S1**. It is noted that the number of surface observational sites established by MEE continuously increased since 2013. We selected these sites with complete records during 2014–2020 for analyzing. Meanwhile, for measurements of the gaseous pollutants after September 2018, we converted the mass concentration under reference state into that under standard state in advance (https://www.mee.gov.cn/xxgk2018/xxgk/xxgk01/201808/t20180815_629602.html).

Moreover, we also obtained the hourly meteorological observation, including surface temperature, relative humidity, and wind speed from the open-source website (<https://q-weather.info/>) for assessing the meteorological conditions in the YRD region. Four meteorological stations located at the provincial cities of the YRD region were collected, including Shanghai, Nanjing, Hangzhou, and Hefei. Illustration of the meteorological stations used in this study is given in **Supplementary Table S2**; **Supplementary Figure S1**.

The WRF-Chem Model

WRF-Chem (Grell et al., 2005) is a regional air quality model developed by the National Center for Atmospheric Research (NCAR), Pacific Northwest National Laboratory (PNNL), and the National Oceanic and Atmospheric Administration (NOAA) of the United States. We applied WRF-Chem (v3.9.1) to simulate the summertime O_3 in July over the YRD region from 2014 to 2020. Each month-long simulation was spinned up for the last 2 days of the previous month. Spatially, two nested domains are configured (Figure 1). The parent domain covers the eastern China (100×100 grid cells) with a horizontal resolution of 18 km. The nested domain,



whose horizontal resolution is 6 km, mainly includes the YRD region (145 × 166 grid cells). A total of 28 vertical layers extends from the ground to the height of 50 hPa. The bottom seven layers distribute below 1 km. The initial and boundary conditions of meteorological fields are determined by FNL reanalysis data sets by the National Centers for Environmental Prediction (NCEP) of the United States. Physical parameterization for describing subgrid processes, such as radiation, microphysics, and the surface layer are listed in **Supplementary Table S3**. For chemical species, the initial and boundary conditions are provided via the global chemical transport model MOZART (Emmons et al., 2010) and CAM-Chem (Emmons et al., 2020). Meanwhile, the Statewide Air Pollution Research Center (SAPRC99) mechanism is utilized for the gas phase reaction scheme in our study (Carter, 2000). For aerosols, we apply Model for Simulating Aerosol Interactions and Chemistry (MOSAIC) as the aerosol parameterization (Zaveri et al., 2008).

Multi-resolution Emission Inventory for China (MEIC) developed by Tsinghua University was adopted as the anthropogenic emission (Li et al., 2017). MEIC summarizes the 0.25° × 0.25° gridded emissions of SO₂, NO_x, CO, CO₂, NH₃, VOCs, EC, OC, PM_{2.5}, and PM₁₀. All species are categorized into five sectors, i.e., agriculture, industry, power, transportation, and residential activities. Online biogenic emissions were calculated by Model of Emissions of Gases and Aerosols from Nature (MEGAN, v2.0.4), which comprehensively took landcover, meteorology, and atmospheric chemical compositions into consideration (Guenther et al., 2006). Biomass burning emissions were provided by the Fire Inventory from NCAR (FINN). Combined with satellite retrieval constrains, FINN can generate high spatio-temporal resolution products of biomass burning emissions (Wiedinmyer et al., 2011).

TABLE 1 | Model performance in predicting meteorological parameters and air pollutants over the YRD region during the study period.

	Mean		IOA	MFB
	Simulation	Observation		
Meteorological parameter				
Temperature (K)	300.2	301.3	0.84	0%
Relative humidity (%)	79.5	79.1	0.85	1%
Wind speed (m·s ⁻¹)	3.1	2.9	0.64	9%
Air pollutant				
PM _{2.5} (μg·m ⁻³)	27.7	29.4	0.59	-17%
NO ₂ (ppb)	14.4	12.6	0.62	12%
O ₃ (ppb)	67.5	51.8	0.66	28%

O₃ Formation Regime

The ratio of formaldehyde (HCHO) to NO_y was utilized as the indicator (i.e., HCHO/NO_y) for diagnosing the formation regime of O₃ (Hu, 2021). In this indicator, HCHO can track the contribution of VOCs (Cao et al., 2018), which is a transient oxidation product of many VOCs and is positively correlated with peroxy radicals. NO_y describes the impacts of multiple reactive nitrogenous compounds, including NO, NO₂, HONO, HNO₃, HO₂NO₂, N₂O₅, NO₃, peroxy acetyl nitrate (PAN), and other organic nitrates. Reactive nitrogen species play a central role in determining the levels of O₃ and hydroxyl radicals in the troposphere. In **Supplementary Figure S2**, NO_y is mainly concentrated in cities along the Yangtze River with 7.2 ppbv on average. Considering that photochemistry is the most active in the presence of abundant radiation, we, thus, investigated the O₃ formation regime from 12:00 to 16:00 (local time, UTC + 8). When HCHO/NO_y is less than 0.3, the O₃ formation regime is considered to be VOC-limited. NO_x controls O₃ production if the ratio is more than 0.72. Otherwise, it is expected to be under a mixed-limited condition, sensitive to changes both in NO_x and

VOCs. The threshold values were obtained by counting the distribution of the HCHO/NO_y for different O₃ formation regimes in the YRD, which allow the HCHO/NO_y sensitivity zone to be delineated in a way that is more consistent with the EKMA curve and accurately represents the sensitivity of O₃ to the precursors (Hu, 2021; Li, 2021).

MODEL EVALUATION

Reliable simulation of meteorological parameters and air pollutants could be the crucial premise for analyzing complicated causes of O₃ pollution. Comparisons between observation versus simulation are concluded in **Table 1**. To statistically quantify the model performance, we applied two following statistical metrics, i.e., index of agreement (IOA, varies from 0 to 1) and mean fractional bias (MFB, varies from -2 to 2). IOA and MFB are calculated based on **Eqs 1–2**, where *s*, *o*, and *N* represent simulation, observation, and the number of samples, respectively.

$$IOA = 1 - \frac{\sum_{i=1}^N (C_s - C_o)^2}{\sum_{i=1}^N \left(\left| C_s - \overline{C_o} \right| + \left| C_o - \overline{C_o} \right| \right)^2} \quad (1)$$

$$MFB = \frac{1}{N} \sum_{i=1}^N \frac{(C_o - C_m)}{\left(\frac{C_o + C_m}{2} \right)} \quad (2)$$

First, our model is capable of reproducing meteorological conditions, which is the key to simulate horizontal transportation, chemical transformation, and the removal of air pollutants. As shown in **Table 1**, the mean observed (simulated) temperature, relative humidity, and wind speed is averaged for 301.3 K (300.2 K), 79.1% (79.5%), and 2.9 m/s (3.1 m/s), respectively, in July from 2014 to 2020. Differences in terms of magnitudes between observation and simulation are quite small. All MFBs are less than 10% as well. IOAs for these meteorological parameters vary from 0.64 to 0.85, highlighting that our model has a good agreement with surface observations. The evaluation indicators of each city for each year can be found in the **Supplementary Table S4**. The city-level IOAs and MFBs varied in 0.6–0.9 and -0.1–0.3 except for the wind speed in 2016, which again confirmed the reasonable model performance.

Moreover, WRF-Chem reasonably reproduced the concentration levels of photochemical products. The mean observed summer O₃ and NO₂ concentrations are 51.8 and 12.6 ppbv averaged for 2014–2020. Simulations for these two species posed an overestimation by 28% and 12%, according to the hourly MFB index. Meanwhile, both hourly IOA values exceed 0.60, indicating that our model reasonably captures the temporal variations of O₃ and NO₂ as well. WRF-Chem also well simulates PM_{2.5} with a predicted IOA of 0.59 as well as a MFB of -17%.

Supplementary Figures S3, S4 show scatterplots of simulations versus observations in daily MDA8 O₃ and NO₂ concentrations and their regression parameters in the 26 cities of the YRD region. The simulated O₃ demonstrates various model performance in different cities. The daily IOA of O₃ ranges from

0.55 (Hefei) to 0.83 (Shanghai) and the corresponding daily MFB poses a range from 13% (Shanghai) to 49% (Wuhu). Meanwhile, most of the fitted slopes of O₃ range from 0.9 to 1.3, further confirming that our model is reliable in reproducing concentrations of O₃. In addition, we verified the diurnal patterns of O₃ in all 26 cities of the YRD region as well. As shown in **Supplementary Figure S5**, both observation and simulation pose the same diurnal patterns with the peak O₃ concentration occurring between 12:00 and 16:00. The correlation coefficients (*R*) are more than 0.96, implying that diurnal variations of O₃ are successfully captured.

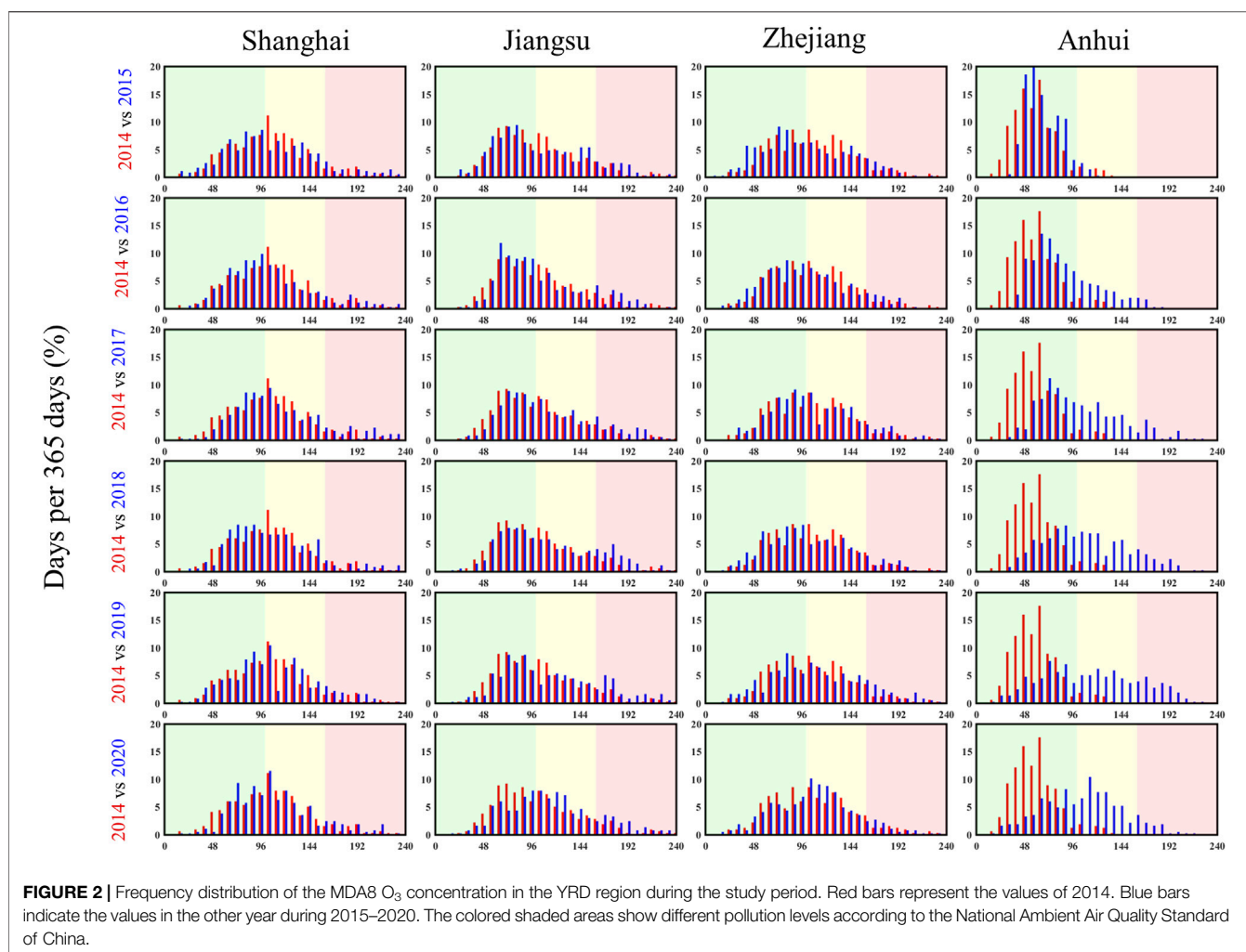
RESULTS AND DISCUSSION

Observed O₃ Pollution in the YRD Region From 2014 to 2020

We first analyzed the observed spatio-temporal variations of six air pollutants over the YRD region from 2014 to 2020. As illustrated in **Supplementary Figure S6**, regional mean O₃ concentration is 107.1 μg m⁻³ in 2020, which increased by 18% compared with the concentration level in 2014. In contrast, concentrations of other five air pollutants sharply decreased over the study period. For example, the annual mean SO₂ shows a dramatic drop by 16.8 μg m⁻³ from 2014 to 2020 with a relative reduction of 68%. At the same time, both PM_{2.5} and PM₁₀ concentrations are also reduced by more than 50%. It is precisely because of this decline that the dominant air pollutant in the YRD region has been changing from PM_{2.5} to O₃. For NO₂, the variation trend generally showed a decrease with a rate of 0.8 μg m⁻³ yr⁻¹ even though an individual slight increase occurred in 2017. The changes of city-level pollutant concentrations are shown in **Supplementary Figure S7**. In addition, **Figure 2; Supplementary Figures S8–S12** show the frequency distribution of O₃, NO₂, PM_{2.5}, PM₁₀, CO, and SO₂ daily concentrations, respectively, which again emphasize that the concentration distribution of O₃ is changing from a low to a high value region while other pollutants show an opposite trend.

Based on the above analysis, we further find that the upward trend of O₃ is significantly different at different stages. In general, the increasing trend of O₃ concentration during 2014–2017 is more obvious in contrast to the years 2018–2020. Annual mean O₃ rapidly increased by 4.9 μg m⁻³ yr⁻¹ (5.5% yr⁻¹) during the period of 2014–2017, while in 2018–2019, the increasing trend slowed down, with the increase rate dropped to 1.1 μg m⁻³ yr⁻¹. Even in 2020, O₃ in many YRD cities has decreased by 0.1–14.3 μg m⁻³ compared with 2019, mainly caused by the reduction of human activity and the more precipitation in 2020, especially in mobile sources and industry (Chen H. et al., 2020; Huang et al., 2021).

In addition, the upward trend of O₃ is also different in different regions of the YRD. As shown in **Figure 3**, the growth of O₃ in the Anhui Province is faster than that in other YRD regions. Especially during 2014–2017, the O₃ concentration in Anhui increased by a rate of 14.7 μg m⁻³ yr⁻¹—four times that in other provinces (i.e., Shanghai, Jiangsu, and Zhejiang, SJZ). Such trends can



also be observed on the city scale (**Supplementary Table S5; Supplementary Figure S7**). Hefei doubled its O₃ concentration between 2014 and 2017 while, in Shanghai, Nanjing, and Hangzhou, the increase was 9.7%–14.3%. To highlight the distinctive variation of O₃ in Anhui, we further compared the frequency distributions of O₃ in Anhui with that in other regions from 2014 to 2020 (**Figure 2**). In 2014, the O₃ concentration in Anhui was mostly concentrated around 50 μg m⁻³ while the city-level O₃ concentration in SJZ distributed in a range of 14.8–256.7 μg m⁻³, and the average value was 80% higher than that in Anhui. However, after 2014, the O₃ in Anhui prominently increased with the frequency distribution rapidly moved to the high value scope (central at ~70 μg m⁻³), and by 2018, it was close to other regions of YRD.

Driving Factors of Interannual Changes in O₃ From 2014 to 2020

We analyze the interannual variation of O₃ in the YRD region from 2014 to 2020 through two factors. One is the O₃ formation regime, and the other is the precursor (NO_x and VOCs) concentrations. The dual role of NO_x in O₃ generation results

in the variation of O₃ formation regime. NO_x can either promote O₃ production through photochemical reactions with atomic oxygen (O), O₂, or mitigate O₃ formation by removing OH from the oxidation cycle. At the same time, ambient radical budget and weather conditions can also affect the O₃ generation regime (Li et al., 2019b; Liu and Wang, 2020a; Lin et al., 2020; Wang et al., 2020).

We employed HCHO/NO_y as an indicator to diagnose the formation regime of O₃. **Figure 4** shows the spatial distributions of the indicator over the YRD region simulated by WRF-Chem. The surrounding areas of the Yangtze River (purple line) are mostly under VOC-limited, mainly due to the abundant NO_x emissions from industrial and shipping activities (An et al., 2021). In contrast, the south regions of YRD demonstrate a universal pattern of NO_x-limited. This could be attributed to the substantial biogenic VOCs emissions from the forest districts in Zhejiang province (Cao et al., 2021). Other YRD regions are mainly controlled by both NO_x and VOCs.

To better understand the fate of O₃ formation regime, we primarily explore the emission characteristics of NO_x and VOCs during this period. As shown in **Figure 5**, the NO_x emission over the YRD region was continuously reduced by a rate of 3.5% yr⁻¹

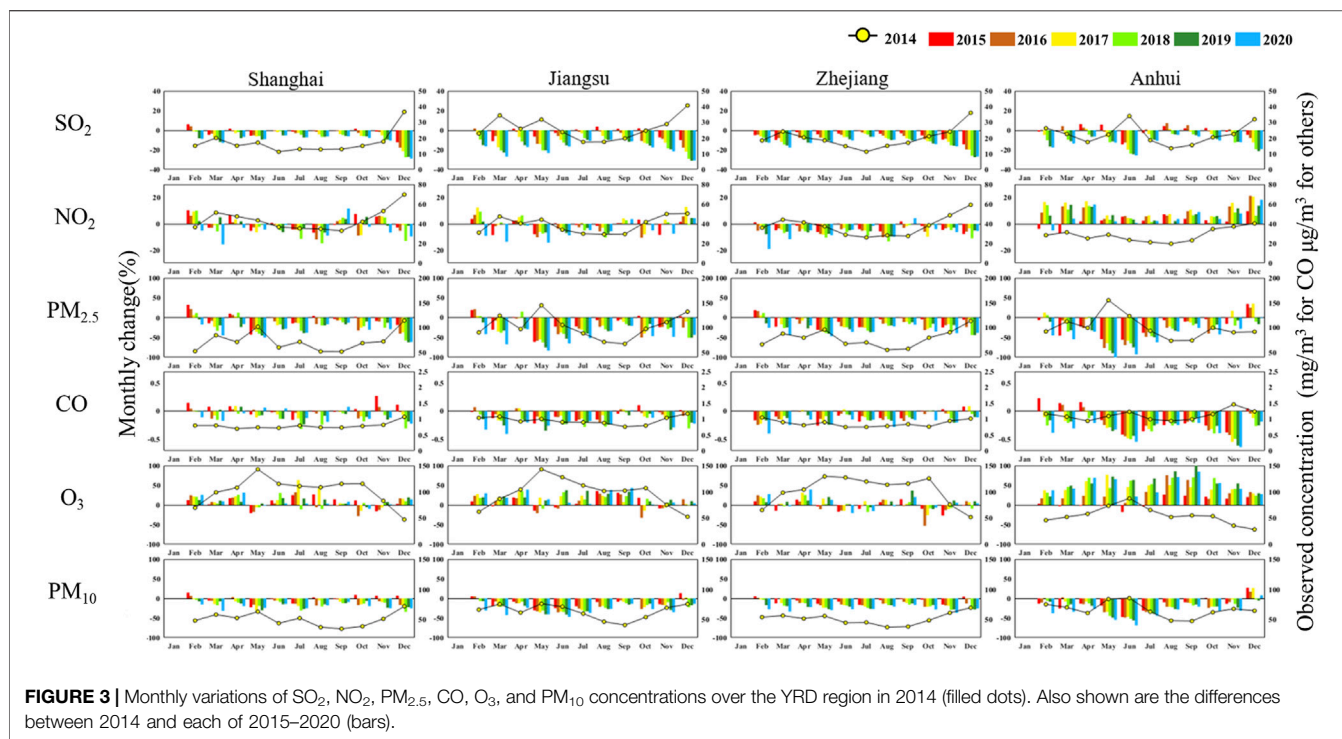


FIGURE 3 | Monthly variations of SO₂, NO₂, PM_{2.5}, CO, O₃, and PM₁₀ concentrations over the YRD region in 2014 (filled dots). Also shown are the differences between 2014 and each of 2015–2020 (bars).

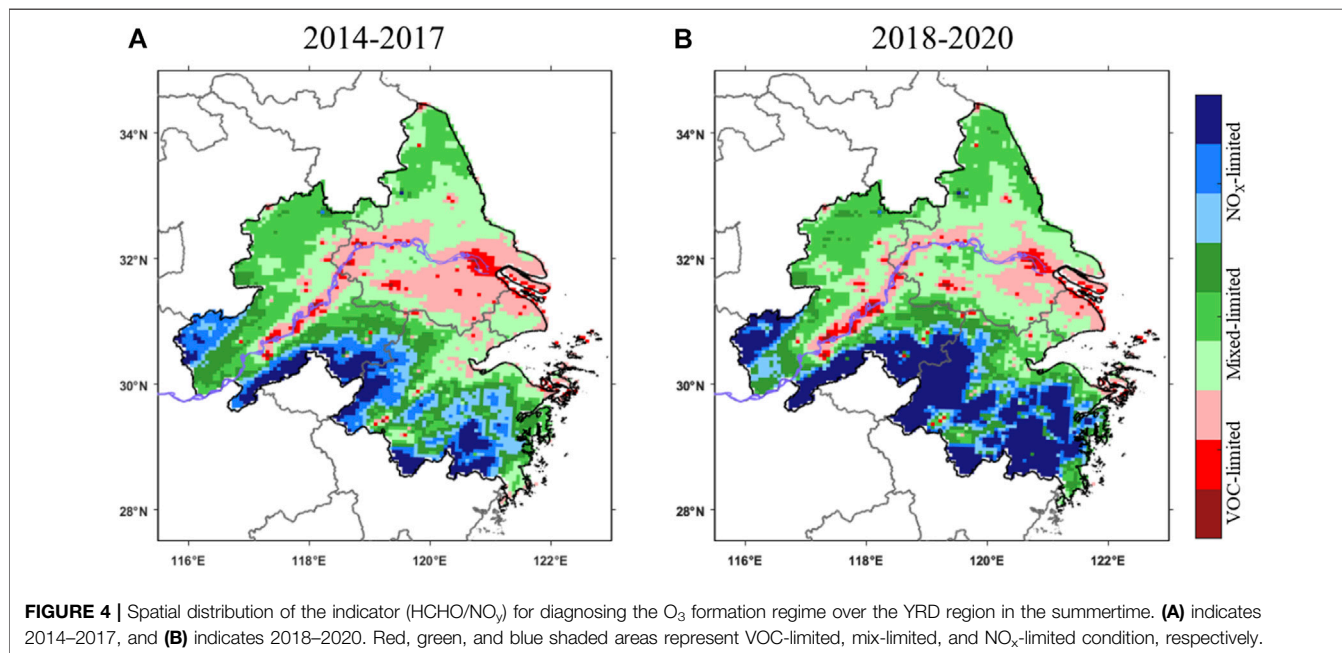
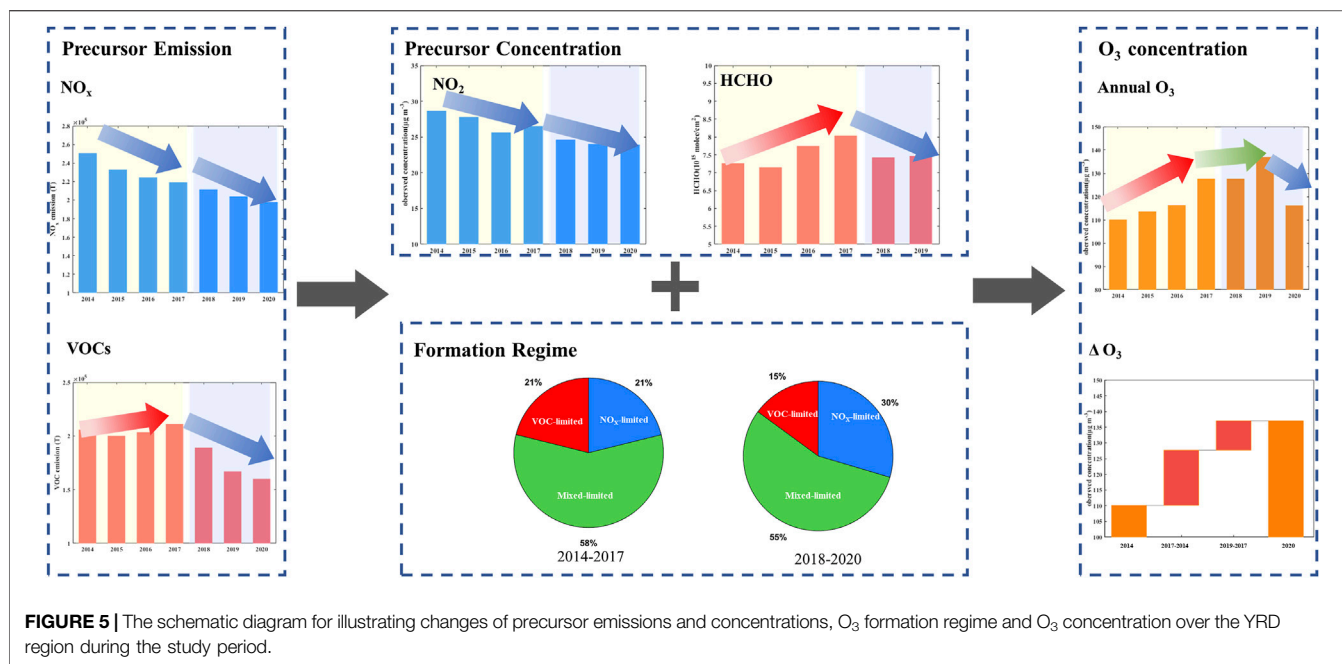


FIGURE 4 | Spatial distribution of the indicator (HCHO/NO_y) for diagnosing the O₃ formation regime over the YRD region in the summertime. (A) indicates 2014–2017, and (B) indicates 2018–2020. Red, green, and blue shaded areas represent VOC-limited, mix-limited, and NO_x-limited condition, respectively.

from 2014 to 2020, which was largely benefited from the APPCAP (http://www.gov.cn/zwgk/2013-09/12/content_2486773.htm). Unprecedented emission reductions due to COVID-19 in 2020 also enhance this trend (Wang G. et al., 2021; Li et al., 2021b; Hu et al., 2021).

However, during 2014 and 2017, the VOC emissions in the YRD region were not effectively controlled and even increased by

0.8% yr⁻¹. After 2018, with the implementation of strict VOC control (http://www.gov.cn/zhengce/content/2018-07/03/content_5303158.htm), VOC emissions began to decline, and in 2020, the VOC emissions in the YRD region dropped by 15.4% compared with the highest level in 2017. The decline in aromatics propene/ethene emission from the petrochemical industry as well as gasoline evaporation and vehicular emissions is the main



component of the reduction of VOCs emissions in 2020 (Wang M. et al., 2021; Qi et al., 2021). The distribution of emission variation also reveals similar trends with the whole region (Supplementary Figure S13). Emissions of NO_x in 2018–2020 decreased by 17.7%–50.8% compared to 2014–2017 in most regions of the YRD. VOCs emissions for 87.8% of YRD areas are reduced in 2018–2020 relative to 2014–2017.

With the changes in NO_x and VOCs emissions, the O₃ formation regime has also changed in response. In 2014–2017, most cities along the Yangtze River are in VOC-limited areas, and other regions are mainly under mix-limited except for the forested areas in southern Zhejiang. Since 2018, the original VOC-limited region has shifted to mix-limited (36%). It should be noted that there are still 15% areas controlled by VOC-limited over the YRD region.

In addition, the concentrations of NO_x and VOCs in the YRD region show a consistent trend as their emissions. As shown in Figure 5, the NO₂ concentration clearly demonstrates a continuous decreasing trend over the YRD region during 2014–2020. In term of VOCs, we employed the column density of HCHO via satellite retrievals to represent the interannual variations of VOCs (Li R. et al., 2021). The column density of HCHO shows an inverted “U” shape, which increases from 7.2×10^{15} molec cm² (2014) to 8.0×10^{15} molec·cm² (2017) and then drops to 7.4×10^{15} molec cm² (2020).

As a result of the changes of both O₃ formation regime and precursor concentrations, the O₃ concentration in the YRD region shows an increasing but variable trend during 2014–2020. Between 2014–2017, the declined NO₂ and the elevated VOCs, under the VOC-limited and mix-limited O₃ formation regime, led to a rapid increase of O₃. However, when it comes to 2018–2020, the VOCs began to slowly

decline, and meanwhile, the formation regime shifted to more mix-limited so that the upward trend of O₃ has obviously slowed down and even appeared as a downward trend in 2020.

Explanation for Distinctive Variation of O₃ in Anhui

The main reason of the rapid growth of O₃ in Anhui, which is different from that in other regions, is the distinctive growth of NO_x during 2014–2017. The NO₂ in Anhui elevated with a rate of $2 \mu\text{g m}^{-3} \text{ yr}^{-1}$ while, in other YRD regions, it posed a remarkable decline of $1.1 \mu\text{g m}^{-3} \text{ yr}^{-1}$. At the same time, the O₃ formation regime in Anhui was mostly controlled by NO_x-limited (24%) or mix-limited conditions (65%). It is also different from other YRD regions where more than 27% areas were controlled by VOC-limited condition. The ambient non-VOC-limited condition is conducive to generation of O₃ when NO₂ increases, via enhancing the “NO_x cycle” (Wang et al., 2017). In addition, the VOCs concentration in Anhui also increased in 2014–2017, which had not yet received much attention over the early stage. It intensified the O₃ production as well. Since 2018, the concentration of O₃ in Anhui ($130.6 \mu\text{g m}^{-3}$) reached the same level as other regions ($122.9 \mu\text{g m}^{-3}$).

DISCUSSION

Though the emission control strategy since 2018 is effective for slowing down the worsening O₃ pollution over the YRD region, there is still a long way to go to see continuous decline in O₃ concentration. Meanwhile, previous studies point out that the O₃ formation regime in other Chinese city clusters, such as the north China plain and PRD, are dominated by VOC-limited and changes toward mix-limited (Jiang et al., 2018; Wang et al.,

2019). To address this issue, a more efficient synergistic measure should be taken to control both NO_x and VOCs (Li et al., 2019c; Huang et al., 2020). O_3 concentration can be quickly reduced with a reasonable reduction ratio between these two precursors according to its nonlinear formation regime. In addition, it is also complicated to conduct the reduction of VOCs emissions. A comprehensive source apportionment for detailed VOCs speciation is necessary for planning better control policies (Wu and Xie, 2017).

Meanwhile, the mitigation of O_3 that is focused on other seasons except for summertime is also proved to be meaningful. Previous case studies of air quality, such as research during COVID-19 or summit exhibited that O_3 could increase resulting from the weakened titration of NO_x due to the reduction of its emissions (Le et al., 2020; Li K. et al., 2021; Zhang et al., 2021b). The elevated O_3 further facilitated the production of secondary aerosols and even led to haze events (Chang et al., 2020; Zhang et al., 2021a; Wang N. et al., 2021). Thus, controlling O_3 concentration during other nonwarm seasons also helps to eliminate the negative environmental impacts by O_3 and $\text{PM}_{2.5}$.

CONCLUSION

In this study, we employed multiple air quality observations and WRF-Chem simulation to describe the increasing but variable trend of O_3 concentration in the YRD region from 2014 to 2020, and further revealed the main factors that caused such trends. During the period of 2014–2020, the annual average O_3 concentration in the YRD region was $101 \mu\text{g m}^{-3}$ with an increase from $93.4 \mu\text{g m}^{-3}$ in 2014 to $107 \mu\text{g m}^{-3}$ in 2020. The increase rate was $4.9 \mu\text{g m}^{-3} \text{ yr}^{-1}$ in the first 4 years, which was four times higher than that in 2018–2020. It should be noted that the O_3 concentration in Anhui significantly increased by $44.1 \mu\text{g m}^{-3}$ during 2014–2017, twofold higher than that in the YRD region ($13.0 \mu\text{g m}^{-3}$). Since 2018, both Anhui and other regions in the YRD slowed down their increase in O_3 .

We further analyzed the two main factors driving the interannual variation of O_3 in the YRD region, including precursor concentrations and the corresponding O_3 formation regime. With the help of the indicator HCHO/NO_y simulated by WRF-Chem, we concluded that the O_3 production regime along the Yangtze River has shifted from VOC-limited to mix-limited.

REFERENCES

- Ainsworth, E. A., Yendrek, C. R., Sitch, S., Collins, W. J., and Emberson, L. D. (2012). The Effects of Tropospheric Ozone on Net Primary Productivity and Implications for Climate Change. *Annu. Rev. Plant Biol.* 63, 637–661. doi:10.1146/annurev-arplant-042110-103829
- An, J., Huang, Y., Huang, C., Wang, X., Yan, R., Wang, Q., et al. (2021). Emission Inventory of Air Pollutants and Chemical Speciation for Specific Anthropogenic Sources Based on Local Measurements in the Yangtze River Delta Region, China. *Atmos. Chem. Phys.* 21 (3), 2003–2025. doi:10.5194/acp-21-2003-2021

In 2014–2017, most cities along the Yangtze River were in VOC-limited areas, and other regions were mainly under mix-limited. After 2018, 36% areas that belong to the VOC-limited condition shifted to a mix-limited condition. Therefore, the alleviative NO_x and elevated VOCs under a VOC- and mix-limited O_3 formation regime generally contributed to the cumulative rise in O_3 concentration. However, since 2018, the drop of both precursors under the mix-limited O_3 formation regime alleviated the worsening O_3 pollution. Our work is of importance to understand the current O_3 pollution in a megacity cluster of China and offers an investigative insight for further alleviating O_3 pollution in the future.

DATA AVAILABILITY STATEMENT

The original contributions presented in the study are included in the article/Supplementary Material, further inquiries can be directed to the corresponding author.

AUTHOR CONTRIBUTIONS

Data curation, model simulation, visualization, and writing-original draft preparation, KT and HZ; Supervision, funding acquisition, writing-review and editing, NL, HL, and JH; Data curation, WF. All authors have read and agreed to the published version of the manuscript.

FUNDING

This work was supported by the National Key Research and Development Program of China (2019YFA0606804), the National Natural Science Foundation of China (41975171), the Major Research Plan of the National Social Science Foundation (18ZDA052).

SUPPLEMENTARY MATERIAL

The Supplementary Material for this article can be found online at: <https://www.frontiersin.org/articles/10.3389/fenvs.2022.836191/full#supplementary-material>

- Barry, V., Klein, M., Winquist, A., Chang, H. H., Mulholland, J. A., Talbott, E. O., et al. (2019). Characterization of the Concentration-Response Curve for Ambient Ozone and Acute Respiratory Morbidity in 5 US Cities. *J. Expo. Sci. Environ. Epidemiol.* 29 (2), 267–277. doi:10.1038/s41370-018-0048-7
- Cao, H., Fu, T.-M., Zhang, L., Henze, D., Miller, C., Lerot, C., et al. (2018). Adjoint Inversion of Chinese Non-methane Volatile Organic Compound Emissions Using Space-Based Observations of Formaldehyde and Glyoxal. *Atmos. Chem. Phys. Discuss.* 18, 1–46. doi:10.5194/acp-2017-1136
- Cao, J., Situ, S., Hao, Y., Xie, S., and Li, L. (2021). Enhanced Summertime Ozone and SOA from Biogenic Volatile Organic Compound (BVOC) Emissions Due to Vegetation Biomass Variability during 1981–2018 in China. *Atmos. Chem. Phys. Discuss.* 2021, 1–21. doi:10.5194/acp-2021-675

- Carter, W. P. L. (2000). *Documentation of the SAPRC-99 Chemical Mechanism for VOC Reactivity Assessment*. California: University of California Riverside. Report to the California Air Resources Board, Contract 92-329. 95-308.
- Chang, Y., Huang, R. J., Ge, X., Huang, X., Hu, J., Duan, Y., et al. (2020). Puzzling Haze Events in China during the Coronavirus (COVID-19) Shutdown. *Geophys. Res. Lett.* 47, e2020GL088533. doi:10.1029/2020GL088533
- Chen, H., Huo, J., Fu, Q., Duan, Y., Xiao, H., and Chen, J. (2020a). Impact of Quarantine Measures on Chemical Compositions of PM_{2.5} during the COVID-19 Epidemic in Shanghai, China. *Sci. Total Environ.* 743, 140758. doi:10.1016/j.scitotenv.2020.140758
- Chen, L., Xing, J., Mathur, R., Liu, S., Wang, S., and Hao, J. (2020b). Quantification of the Enhancement of PM_{2.5} Concentration by the Downward Transport of Ozone from the Stratosphere. *Chemosphere* 255, 126907. doi:10.1016/j.chemosphere.2020.126907
- Chen, L., Zhu, J., Liao, H., Yang, Y., and Yue, X. (2020c). Meteorological Influences on PM_{2.5} and O₃ Trends and Associated Health Burden since China's Clean Air Actions. *Sci. Total Environ.* 744, 140837. doi:10.1016/j.scitotenv.2020.140837
- Chen, X., Jiang, Z., Shen, Y., Li, R., Fu, Y., Liu, J., et al. (2021). Chinese Regulations Are Working—Why Is Surface Ozone over Industrialized Areas Still High? Applying Lessons from Northeast US Air Quality Evolution. *Geophys. Res. Lett.* 48 (14), e2021GL092816. doi:10.1029/2021gl092816
- Dang, R., Liao, H., and Fu, Y. (2021). Quantifying the Anthropogenic and Meteorological Influences on Summertime Surface Ozone in China over 2012–2017. *Sci. Total Environ.* 754, 142394. doi:10.1016/j.scitotenv.2020.142394
- Eklund, J., Olsson, D., Forsberg, B., Andersson, C., and Orru, H. (2021). The Effect of Current and Future Maternal Exposure to Near-Surface Ozone on Preterm Birth in 30 European Countries—An EU-wide Health Impact Assessment. *Environ. Res. Lett.* 16 (5). doi:10.1088/1748-9326/abe6c4
- Emmons, L. K., Schwantes, R. H., Orlando, J. J., Tyndall, G., Kinnison, D., Lamarque, J.-F., et al. (2020). The Chemistry Mechanism in the Community Earth System Model Version 2 (CESM2). *J. Adv. Model. Earth Syst.* 12 (4), e2019MS001882. doi:10.1029/2019MS001882
- Emmons, L. K., Walters, S., Hess, P. G., Lamarque, J. F., Pfister, G. G., Fillmore, D., et al. (2010). Description and Evaluation of the Model for Ozone and Related Chemical Tracers, Version 4 (MOZART-4). *Geosci. Model. Dev.* 3 (1), 43–67. doi:10.5194/gmd-3-43-2010
- Feng, T., Zhao, S., Bei, N., Liu, S., and Li, G. (2021). Increasing Atmospheric Oxidizing Capacity Weakens Emission Mitigation Effort in Beijing during Autumn Haze Events. *Chemosphere* 281, 130855. doi:10.1016/j.chemosphere.2021.130855
- Feng, Z., Hu, E., Wang, X., Jiang, L., and Liu, X. (2015). Ground-level O₃ Pollution and its Impacts on Food Crops in China: a Review. *Environ. Pollut.* 199, 42–48. doi:10.1016/j.envpol.2015.01.016
- Grell, G. A., Peckham, S. E., Schmitz, R., McKeen, S. A., Frost, G., Skamarock, W. C., et al. (2005). Fully Coupled “Online” Chemistry within the WRF Model. *Atmos. Environ.* 39 (37), 6957–6975. doi:10.1016/j.atmosenv.2005.04.027
- Guan, Y., Xiao, Y., Wang, F., Qiu, X., and Zhang, N. (2021). Health Impacts Attributable to Ambient PM_{2.5} and Ozone Pollution in Major Chinese Cities at Seasonal-Level. *J. Clean. Prod.* 311, 127510. doi:10.1016/j.jclepro.2021.127510
- Guenther, A., Karl, T., Harley, P., Wiedinmyer, C., Palmer, P. I., and Geron, C. (2006). Estimates of Global Terrestrial Isoprene Emissions Using MEGAN (Model of Emissions of Gases and Aerosols from Nature). *Atmos. Chem. Phys.* 6 (11), 3181–3210. doi:10.5194/acp-6-3181-2006
- Hu, J. (2021). “Exploring the Applicability of Indicators for Determining Ozone Sensitivity (In Chinese),” in *The 3rd Workshop on Atmospheric Ozone Pollution Prevention and Control in China* (Shanghai, China: Chinese Society For Environmental Sciences).
- Hu, X., Liu, Q., Fu, Q., Xu, H., Shen, Y., Liu, D., et al. (2021). A High-Resolution Typical Pollution Source Emission Inventory and Pollution Source Changes during the COVID-19 Lockdown in a Megacity, China. *Environ. Sci. Pollut. Res. Int.* 28 (33), 45344–45352. doi:10.1007/s11356-020-11858-x
- Huang, C., An, J., Wang, H., Liu, Q., Tian, J., Wang, Q., et al. (2021). Highly Resolved Dynamic Emissions of Air Pollutants and Greenhouse Gas CO₂ during COVID-19 Pandemic in East China. *Environ. Sci. Technology Lett.* 8 (10), 853–860. doi:10.1021/acs.estlett.1c00600
- Huang, X., Ding, A., Gao, J., Zheng, B., Zhou, D., Qi, X., et al. (2020). Enhanced Secondary Pollution Offset Reduction of Primary Emissions during COVID-19 Lockdown in China. *Natl. Sci. Rev.* 8 (2), nwaal37. doi:10.1093/nsr/nwaa137
- Jiang, M., Lu, K., Su, R., Tan, Z., Wang, H., Li, L., et al. (2018). Ozone Formation and Key VOCs in Typical Chinese City Clusters. *Chin. Sci. Bull.* 63 (12), 1130–1141. doi:10.1360/n972017-01241
- Le, T., Wang, Y., Liu, L., Yang, J., Yung, Y. L., Li, G., et al. (2020). Unexpected Air Pollution with Marked Emission Reductions during the COVID-19 Outbreak in China. *Science* 369 (6504), 702–706. doi:10.1126/science.abb7431
- Lei, R., Zhu, F., Cheng, H., Liu, J., Shen, C., Zhang, C., et al. (2019). Short-term Effect of PM_{2.5}/O₃ on Non-accidental and Respiratory Deaths in Highly Polluted Area of China. *Atmos. Pollut. Res.* 10 (5), 1412–1419. doi:10.1016/j.apr.2019.03.013
- Li, K., Jacob, D. J., Liao, H., Qiu, Y., Shen, L., Zhai, S., et al. (2021a). Ozone Pollution in the North China Plain Spreading into the Late-winter Haze Season. *Proc. Natl. Acad. Sci. U S A.* 118 (10), e2015797118. doi:10.1073/pnas.2015797118
- Li, K., Jacob, D. J., Liao, H., Shen, L., Zhang, Q., and Bates, K. H. (2019a). Anthropogenic Drivers of 2013–2017 Trends in Summer Surface Ozone in China. *Proc. Natl. Acad. Sci.* 116 (2), 422–427. doi:10.1073/pnas.1812168116
- Li, K., Jacob, D. J., Liao, H., Shen, L., Zhang, Q., and Bates, K. H. (2019b). Anthropogenic Drivers of 2013–2017 Trends in Summer Surface Ozone in China. *Proc. Natl. Acad. Sci. U S A.* 116 (2), 422–427. doi:10.1073/pnas.1812168116
- Li, K., Jacob, D. J., Liao, H., Zhu, J., Shah, V., Shen, L., et al. (2019c). A Two-Pollutant Strategy for Improving Ozone and Particulate Air Quality in China. *Nat. Geosci.* 12, 906–910. doi:10.1038/s41561-019-0464-x
- Li, M., Wang, T., Xie, M., Li, S., Zhuang, B., Fu, Q., et al. (2021b1994). Drivers for the Poor Air Quality Conditions in North China Plain during the COVID-19 Outbreak. *Atmos. Environ.* 246, 118103. doi:10.1016/j.atmosenv.2020.118103
- Li, M., Zhang, Q., Kurokawa, J. I., Woo, J. H., He, K., Lu, Z., et al. (2017). MIX: a Mosaic Asian Anthropogenic Emission Inventory under the International Collaboration Framework of the MICS-Asia and HTAP. *Atmos. Chem. Phys.* 17 (2), 935–963. doi:10.5194/acp-17-935-2017
- Li, R., Xu, M., Li, M., Chen, Z., Zhao, N., Gao, B., et al. (2021c). Identifying the Spatiotemporal Variations in Ozone Formation Regimes across China from 2005 to 2019 Based on Polynomial Simulation and Causality Analysis. *Atmos. Chem. Phys.* 21 (20), 15631–15646. doi:10.5194/acp-21-15631-2021
- Li, X. (2021). *Research On the Applicability of Ozone Sensitivity Determination Indicators in Jiangsu*. Master. Nanjing: Nanjing University of Information Science & Technology.
- Lin, H., Wang, M., Duan, Y., Fu, Q., Ji, W., Cui, H., et al. (2020). O₃ Sensitivity and Contributions of Different NMHC Sources in O₃ Formation at Urban and Suburban Sites in Shanghai. *Atmosphere* 11 (3), 295. doi:10.3390/atmos11030295
- Liu, H., Liu, J., Liu, Y., Yi, K., Yang, H., Xiang, S., et al. (2021). Spatiotemporal Variability and Driving Factors of Ground-Level Summertime Ozone Pollution over Eastern China. *Atmos. Environ.* 265, 118686. doi:10.1016/j.atmosenv.2021.118686
- Liu, Y., and Wang, T. (2020a). Worsening Urban Ozone Pollution in China from 2013 to 2017 – Part 1: The Complex and Varying Roles of Meteorology. *Atmos. Chem. Phys.* 20 (11), 6305–6321. doi:10.5194/acp-20-6305-2020
- Liu, Y., and Wang, T. (2020b). Worsening Urban Ozone Pollution in China from 2013 to 2017 – Part 2: The Effects of Emission Changes and Implications for Multi-Pollutant Control. *Atmos. Chem. Phys.* 20 (11), 6323–6337. doi:10.5194/acp-20-6323-2020
- Mousavinezhad, S., Choi, Y., Pouyaei, A., Ghahremanloo, M., and Nelson, D. L. (2021). A Comprehensive Investigation of Surface Ozone Pollution in China, 2015–2019: Separating the Contributions from Meteorology and Precursor Emissions. *Atmos. Res.* 257, 105599. doi:10.1016/j.atmosres.2021.105599
- Qi, J., Mo, Z., Yuan, B., Huang, S., Huangfu, Y., Wang, Z., et al. (2021). An Observation Approach in Evaluation of Ozone Production to Precursor Changes during the COVID-19 Lockdown. *Atmos. Environ.* 262, 118618. doi:10.1016/j.atmosenv.2021.118618
- Seinfeld, J. H., and Pandis, S. N. (2006). *Atmospheric Chemistry and Physics: From Air Pollution to Climate Change*. Third edition. New York: John Wiley.
- Shen, F., Zhang, L., Jiang, L., Tang, M., Gai, X., Chen, M., et al. (2020). Temporal Variations of Six Ambient Criteria Air Pollutants from 2015 to 2018, Their Spatial Distributions, Health Risks and Relationships with Socioeconomic Factors during 2018 in China. *Environ. Int.* 137, 105556. doi:10.1016/j.envint.2020.105556

- Shen, L., Jacob, D. J., Liu, X., Huang, G., Li, K., Liao, H., et al. (2019). An Evaluation of the Ability of the Ozone Monitoring Instrument (OMI) to Observe Boundary Layer Ozone Pollution across China: Application to 2005–2017 Ozone Trends. *Atmos. Chem. Phys.* 19 (9), 6551–6560. doi:10.5194/acp-19-6551-2019
- Thompson, A. M. (1992). The Oxidizing Capacity of the Earth's Atmosphere: Probable Past and Future Changes. *Science* 256 (5060), 1157–1165. doi:10.1126/science.256.5060.1157
- Wang, G., Huang, K., Fu, Q., Chen, J., Huo, J., Zhao, Q., et al. (2021a). Response of PM_{2.5}-bound Elemental Species to Emission Variations and Associated Health Risk Assessment during the COVID-19 Pandemic in a Coastal Megacity. *J. Environ. Sci.* 122, 115–127. doi:10.1016/j.jes.2021.10.005
- Wang, G., Jia, S., Li, R., Ma, S., Chen, X., Wu, Z., et al. (2020). Seasonal Variation Characteristics of Hydroxyl Radical Pollution and its Potential Formation Mechanism during the Daytime in Lanzhou. *J. Environ. Sci.* 95, 58–64. doi:10.1016/j.jes.2020.03.045
- Wang, M., Lu, S., Shao, M., Zeng, L., Zheng, J., Xie, F., et al. (2021b). Impact of COVID-19 Lockdown on Ambient Levels and Sources of Volatile Organic Compounds (VOCs) in Nanjing, China. *Sci. Total Environ.* 757, 143823. doi:10.1016/j.scitotenv.2020.143823
- Wang, N., Lyu, X., Deng, X., Huang, X., Jiang, F., and Ding, A. (2019). Aggravating O₃ Pollution Due to NO_x Emission Control in Eastern China. *Sci. Total Environ.* 677, 732–744. doi:10.1016/j.scitotenv.2019.04.388
- Wang, N., Xu, J., Pei, C., Tang, R., Zhou, D., Chen, Y., et al. (2021c). Air Quality during COVID-19 Lockdown in the Yangtze River Delta and the Pearl River Delta: Two Different Responsive Mechanisms to Emission Reductions in China. *Environ. Sci. Technol.* 55 (9), 5721–5730. doi:10.1021/acs.est.0c08383
- Wang, T., Xue, L., Brimblecombe, P., Lam, Y. F., Li, L., and Zhang, L. (2017). Ozone Pollution in China: A Review of Concentrations, Meteorological Influences, Chemical Precursors, and Effects. *Sci. Total Environ.* 575, 1582–1596. doi:10.1016/j.scitotenv.2016.10.081
- Wiedinmyer, C., Akagi, S. K., Yokelson, R. J., Emmons, L. K., Al-Saadi, J. A., Orlando, J. J., et al. (2011). The Fire INventory from NCAR (FINN): a High Resolution Global Model to Estimate the Emissions from Open Burning. *Geoscientific Model. Development* 4 (3), 625–641. doi:10.5194/gmd-4-625-2011
- Wu, R., and Xie, S. (2017). Spatial Distribution of Ozone Formation in China Derived from Emissions of Speciated Volatile Organic Compounds. *Environ. Sci. Technol.* 51 (5), 2574–2583. doi:10.1021/acs.est.6b03634
- Zaveri, R. A., Easter, R. C., Fast, J. D., and Peters, L. K. (2008). Model for Simulating Aerosol Interactions and Chemistry (MOSAIC). *J. Geophys. Res.* 113 (D13). doi:10.1029/2007jd008782
- Zhai, S., Jacob, D. J., Wang, X., Shen, L., Li, K., Zhang, Y., et al. (2019). Fine Particulate Matter (PM_{2.5}) Trends in China, 2013–2018: Separating Contributions from Anthropogenic Emissions and Meteorology. *Atmos. Chem. Phys.* 19 (16), 11031–11041. doi:10.5194/acp-19-11031-2019
- Zhang, H., Li, N., Tang, K., Liao, H., Shi, C., Huang, C., et al. (2021a). Estimation of Secondary PM_{2.5} in China and the United States Using a Multi-Tracer Approach. *Atmos. Chem. Phys. Discuss.* 2021, 1–36. doi:10.5194/acp-2021-683
- Zhang, H., Tang, K., Feng, W., Yan, X., Liao, H., and Li, N. (2021b). Impact of Short-Term Emission Control Measures on Air Quality in Nanjing during the Jiangsu Development Summit. *Front. Environ. Sci.* 9, 693513. doi:10.3389/fenvs.2021.693513
- Zheng, B., Tong, D., Li, M., Liu, F., Hong, C., Geng, G., et al. (2018). Trends in China's Anthropogenic Emissions since 2010 as the Consequence of Clean Air Actions. *Atmos. Chem. Phys.* 18 (19), 14095–14111. doi:10.5194/acp-18-14095-2018

Conflict of Interest: The authors declare that the research was conducted in the absence of any commercial or financial relationships that could be construed as a potential conflict of interest.

Publisher's Note: All claims expressed in this article are solely those of the authors and do not necessarily represent those of their affiliated organizations, or those of the publisher, the editors, and the reviewers. Any product that may be evaluated in this article or claim that may be made by its manufacturer, is not guaranteed or endorsed by the publisher.

Copyright © 2022 Tang, Zhang, Feng, Liao, Hu and Li. This is an open-access article distributed under the terms of the Creative Commons Attribution License (CC BY). The use, distribution or reproduction in other forums is permitted, provided the original author(s) and the copyright owner(s) are credited and that the original publication in this journal is cited, in accordance with accepted academic practice. No use, distribution or reproduction is permitted which does not comply with these terms.